Research Article | Vol. 29, No. 23 / 8 Nov 2021 / Optics Express 38095
Optics EXPRESS

Multipole-phase division multiplexing

GIANLUCA RUFFATO,[1,2,*] VINCENZO GRILLO,[3] AND FILIPPO ROMANATO[1,2,4]

[1]Department of Physics and Astronomy 'G. Galilei', University of Padova, via Marzolo 8, 35131 Padova, Italy
[2]Padua Quantum Technologies Research Center, University of Padova, via Gradenigo 6, Padova, Italy
[3]CNR-Istituto Nanoscienze, Centro S3, Via G Campi 213/a, I-41125 Modena, Italy
[4]CNR-IOM Istituto Officina Molecolare, S.S. 14 - Km. 163,5 - 34149 Trieste (TS), Italy
*gianluca.ruffato@unipd.it

Abstract: The control of structured waves has recently opened innovative scenarios in the perspective of radiation propagation, advanced imaging, and light-matter interaction. In information and communication technology, the spatial degrees of freedom offer a wider state space to carry many channels on the same frequency or increase the dimensionality of quantum protocols. However, spatial decomposition is much more arduous than polarization or frequency multiplexing, and very few practical examples exist. Among all, beams carrying orbital angular momentum gained a preeminent role, igniting a variety of methods and techniques to generate, tailor, and measure that property. In a more general insight into structured-phase beams, we introduce here a new family of wave fields having a multipole phase. These beams are devoid of phase singularities and described by two continuous spatial parameters which can be controlled in a practical and compact way via conformal optics. The outlined framework encompasses multiplexing, propagation, and demultiplexing as a whole for the first time, describing the evolution and transformation of wave fields in terms of conformal mappings. With its potentialities, versatility, and ease of implementation, this new paradigm introduces a novel playground for space division multiplexing, suggesting unconventional solutions for light processing and free-space communications.

1. Introduction

A deeper insight into the nature and properties of light has always driven technological advances and inspired disruptive applications. In fact, the exploitation of a particular property demands methods and components for the manipulation of that specific feature. With the flourishing of research and applications on structured light [1], the necessity to customize the intensity and phase distribution of a beam pursued the ability to process the wave fields analogously to spectral or polarization decomposition. However, while the latter operations can be done straightforwardly, spatial decomposition is practically more demanding and few examples exist. Some classes of beams have been identified in order to describe the proper method to perform spatial decomposition for specific issues: Hermite- and Laguerre-Gaussian [2], Bessel [3], Elegant beams [4] are among the most famous. The exploration of these beam families and of their spatial degrees of freedom as control and manipulation parameters has paved the way to formidable milestones in a variety of fields, such as microscopy and imaging [5–7], micromanipulation [8,9], and information and communication technology [10–13]. In the last field in particular [14], the possibility to access a wider state space enabled disruptive applications for high-capacity classical links [15–17] and high-dimensional quantum key distribution [18].

So far, a preeminent role has been played by beams carrying orbital angular momentum (OAM) [19–21], endowed with an azimuthal phase term $exp(i\ell\vartheta)$, and the research on their generation and control has inspired the development of a rich portfolio of techniques with various levels of

#438898 https://doi.org/10.1364/OE.438898
Journal © 2021 Received 27 Jul 2021; revised 25 Sep 2021; accepted 6 Oct 2021; published 1 Nov 2021

Optics EXPRESS

complexity, efficiency, and miniaturization [22–37]. Among all, conformal mappings outline two-element architectures to perform efficiently the generation, manipulation, and sorting in a versatile and scalable way [38]. The so-called *log-pol* mapping [27], transforming an azimuthal phase gradient into a linear one, provided a solution for OAM measurement (demultiplexing) [28,29] and generation (multiplexing) [30–32] by moving those operations to plane waves, being much easier to process using a common Fourier lens. The *spiral transformation* has been introduced to increase the resolution in demultiplexing [33], and its recent evolution has been demonstrated to perform the arbitrary multiplication and division of OAM [34]. The same operations have been lately achieved by splitting and mapping the azimuthal phase gradient onto complementary circular sectors (multiplication) or distinct intensity rings (division). Those operations can be performed by properly combining and engineering a subset of the so-called *circular-sector transformations* [36,37].

In a more general approach to the propagation of structured-phase beams, we show here how circular-sector transformations transcend the realm of optical vortices and configure an efficient method for the generation and measurement of new families of wave fields, hereafter referred to as multipole-phase beams. With respect to OAM beams, these solutions can be devoid of phase singularities and their harmonic phase patterns are described by two continuous parameters, i.e., the phase strength and orientation angle, defining the modulus and rotation of the phase pattern on a plane perpendicular to the propagation direction, respectively. Circular-sector transformations are demonstrated to perform the mapping between multipole phases and linear phase gradients,

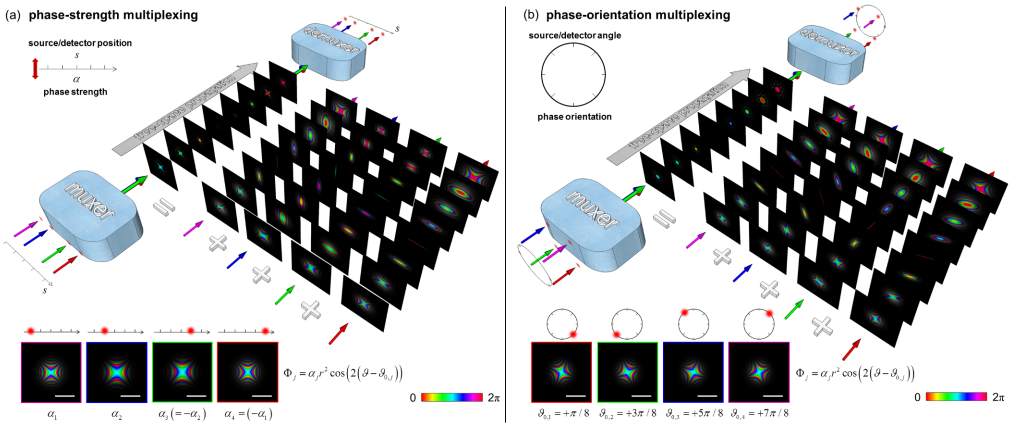

Fig. 1. Scheme of multipole-phase division multiplexing working principle for the specific case of multipole order equal to +2. A linear (a) and a circular (b) distribution of independent Gaussian beams are first multiplexed into a set of superimposed beams with multipole phases, then demultiplexed after transmission. The two schemes can be used in combination and are here shown separately only for the sake of clarity. The multipole phase term of the jth beam is given by $\Phi_j=\alpha_j r^2\cos(2(\vartheta-\vartheta_{0,j}))$, defined by the phase strength α_j and orientation angle $\vartheta_{0,j}$. The modulation of these two degrees of freedom offers a 2D dense space (α_j, $\vartheta_{0,j}$) over which the information channels can be multiplexed and demultiplexed at the same frequency. The (de)multiplexing devices allow to conjugate the two parameters to the axial displacement and orientation of the jth input/output beam, respectively. (a) Phase-strength multiplexing: beams carrying different phase strengths $\{\alpha_j\}$ are conjugated to distinct axial positions proportional to α_j. (b) Phase-orientation multiplexing: beams with the same phase strength and different orientation angles $\{\vartheta_{0,j}\}$ are conjugated to distinct angular positions $\{-2\cdot\vartheta_{0,j}\}$ of the (de)multiplexed beams on the same circle. The intensity/phase patterns show the numerical propagation in free space over 300 m at 632.8 nm. Brightness and colors refer to intensity and phase, respectively. (a, b) Scale bars on the bottom-left fields: 4 cm.

Optics EXPRESS

which can be more easily generated and sorted with a lens. This suggests an efficient and compact method for the (de)multiplexing of those beams onto a 2D constellation of sources or detectors. Moreover, the preservation of a multipole-phase structure under Fourier transform supports the validity of those beams for applications to spatial division multiplexing.

The present research paves the way to a novel paradigm for spatial division multiplexing, hereafter called multipole-phase division multiplexing (Fig. 1). The underlying theory and experimental results lay the foundation of a complete framework including as a whole, for the first time, the operations of generation, transmission, and measurement of spatial configurations of the electromagnetic fields in terms of conformal mappings. This is expected to find promising applications especially for free-space transmission, from the optical up to the microwave and radio regimes.

2. Theory and simulation

As depicted in Fig. 1, the basic idea of spatial division multiplexing with multipole-phase beams is to transform a linear or a circular distribution of (Gaussian) beams in a superposition of multipole-phase beams (multiplexing) and, after propagation, to perform the backward transformation to the original distribution (demultiplexing). The phase pattern of this new type of beams is described by two continuous parameters, defining the phase gradient and the angular orientation, which are put in one-to-one correspondence to the radial and angular positions of a 2D constellation of lasers and detectors, at the transmitter and the receiver sides, respectively. In the following, we provide a derivation of the underlying theoretical background, referring to Supplement 1 for more detailed calculations.

In the paraxial regime, the propagation in free-space of an initial field of complex amplitude $U^{(i)}(r, \vartheta)=u^{(i)}(r, \vartheta)e^{i\Omega(r,\vartheta)}$ is described by the Fresnel diffraction integral [39]:

$$U(\rho, \varphi, z) = \frac{e^{ikz}}{i\lambda z} e^{ik\frac{\rho^2}{2z}} \iint u^{(i)}(r, \vartheta) e^{i\Omega(r,\vartheta)} e^{ik\frac{r^2}{2z}} e^{-ik\frac{r\rho}{z}\cos(\vartheta-\varphi)} r dr d\vartheta. \tag{1}$$

If a quadratic term $\Omega_f=-kr^2/(2f)$ is included, then the field in $z=f$ is proportional to the Fourier transform of the input one. The stationary phase approximation [40,41] represents a useful tool to solve an integral of this type, by approximating it with the values of the argument at the stationary points of the total phase. From a physical point of view, the approximation is equivalent to a ray-light approach to the problem, suggesting that the energy at the input point (ρ, φ) is sent to the point in $z=f$ given by:

$$\rho = \frac{f}{k} \nabla\Omega|_{\mathbf{r}}, \tag{2}$$

being $\nabla\Omega|_{\boldsymbol{r}}/k$ the inclination angle of the ray emerging from the point $\boldsymbol{r}=(r, \vartheta)$. This can be thought of as a coordinate change $\boldsymbol{\rho}\equiv \boldsymbol{\rho}(r, \vartheta)$ induced by the input phase term Ω. In the quest of a phase structure to be exploited for space division multiplexing, we consider a phase pattern imparting a transformation that is conformal, i.e., it locally conserves the angles. Under this constrain, it is straightforward to show (see Supplement 1 S1) that the phase Ω must be harmonic, i.e., it satisfies Laplace's equation $\nabla^2\Omega=0$, whose general solution under variable separation is given by:

$$\Omega(r, \vartheta) = \alpha r^m \cos(m(\vartheta - \vartheta_0)). \tag{3}$$

Due to the analogy with the integrated fields of multipoles in electrostatics [42], we will refer to a phase pattern as that in Eq. (3) as a multipole phase, being α and ϑ_0 continuous parameters describing the phase strength and orientation, respectively. The beams families are identified by the parameter m that measures the multiplicity order. For $m>0$, the phase in Eq. (3) is defined over the whole plane (r, ϑ), therefore it does not introduce points of null intensity associated to phase singularities or discontinuities. In general, under free-space propagation, a field with

Optics EXPRESS

multipole phase of order m is Fourier transformed into a multipole phase of order $m/(m\text{-}1)$, with phase strength and orientation depending on the input values (see Supplement 1).

With the aim to exploit those beams for structured light applications, it becomes essential to find out, for each order m, an effective method to generate and sort the multipole phases on the basis of their defining parameters α and ϑ_0. Analogous to the role of *log-pol* transformation for OAM beams, the idea is to find out a mapping between multipole phases and linear phase gradients, which can be easily multiplexed or separated by means of a Fourier lens. In the case of multipole-phase beams, this is achieved by implementing an n-fold circular-sector transformation [36] with factor n=-1/m, mapping conformally a point (r,ϑ) to the new polar coordinates $(\rho,\varphi)=(a(r/b)^{-1/n}, \vartheta/n))=(a(r/b)^m, -m\vartheta)$, being a and b arbitrary scaling parameters. The transformation performs substantially a scaling on the azimuthal coordinate, while the power scaling on the radial coordinate is dictated by the Cauchy-Riemann conditions that a conformal mapping must satisfy [40]. Under this transformation, the phase in Eq. (3) is transformed into the linear phase gradient:

$$\Phi^{out}(\rho,\varphi) = \beta\rho\cos(\varphi-\varphi_0), \tag{4}$$

with the definitions $\beta=\alpha b^m/a$ and $\varphi_0=-m\vartheta_0$. As shown in [36,37] (see Supplement 1 S2 for detailed calculations), a circular-sector transformation with factor n=-1/m is imparted by a phase-only element with transmission function equal to $exp(i\Omega^{D}{}_{m,1})$, where

$$\Omega^{D}_{m,1}(r,\vartheta) = K\cdot r^{1+m}\cos((1+m)\vartheta), \tag{5}$$

and $K=kab^{-m}/((1+m)f)$. Actually, a further confocal phase plate is required in $z=f$ to complete the phase transformation, accounting for the phase distortions due to the in-between propagation. This second element exhibits a phase $\Omega^{D}{}_{m,2}$ with the same functional dependence as that in Eq. (5), under the substitutions $m\rightarrow 1/m$ and $a\leftrightarrow b$ (plus a quadratic focusing to introduce a Fresnel correction). As a matter of fact, this element performs the inverse transformation when the optical system is illuminated in reverse, i.e., a circular-sector transformation by a scaling factor $1/n$ (=-m).

Comparing Eq. (5) and Eq. (3), it is worth noting that the two elements required to process the multipole order m, are endowed with multipole phases as well, of orders $1+m$ and $1+1/m$, respectively. Hence, the concept of *multipole phase* encompasses the description of both the structured beams and the phase patterns that are necessary for their optical processing, and a precise relation exists between their different multipole orders.

After placing a lens in cascade to the second element in *f-f* configuration, a bright spot is expected on its back focal plane at the polar coordinates:

$$(R,\theta) = \left(\frac{f_F}{k}\beta,\varphi_0\right) = \left(\frac{f_F}{k}\frac{\alpha b^m}{a}, -m\vartheta_0\right), \tag{6}$$

being f_F the focal length of the Fourier lens. Therefore, beams endowed with multipole phases of the same order m, but with different strength and orientation values, can be mapped onto distinct points in far field by using the sequence of an n-fold circular-sector transformation with n=-1/m and a Fourier lens.

Conversely, the same configuration can be used to multiplex several input beams into a collimated bunch of multipole phases with the same order m but different phase strengths and orientations. Actually, the first element is not exactly as the second one in the demultiplexer. As a matter of fact, since the inverse transformation performs the mapping of the whole pattern onto a circular sector with amplitude $2\pi/|m|$, an additional $|m|$-fold multiplication is needed in order to obtain a beam defined over the whole 2π range. Therefore, the required phase turns out to be the combination of $|m|$ phase patterns performing (-m)-fold circular-sector transformations, rotated of $2\pi/|m|$ with respect to each other (Supplement 1 S3).

Optics EXPRESS

In order to prove the working principle of multipole-phase beams transformation, we will focus our analysis on the specific case m=+2. The importance of this order is dictated by its invariance under Fourier transform, i.e., paraxial free-space propagation, since it is the unique non-trivial solution of the condition $m = m/(m\text{-}1)$. However, this choice allows one to describe the characteristic properties of multipole-phase beams without any loss of generality. For the sake of clarity, we will focus specifically on the demultiplexing stage, due to the symmetry of the backward process (multiplexing) under time reversal.

The demultiplexing scheme is depicted in Fig. 2, where the input field is mapped onto a linear phase gradient by means of a circular-sector transformation with n=-1/2 and sorted by a Fourier lens in cascade. The phase patterns of the required optical elements are obtained by substituting m=+2 and m=+1/2 in Eq. (3), plus quadratic terms for focusing and Fresnel correction. Their phase patterns are shown in Figs. 2(b) and 2(c) (without the quadratic terms). A numerical simulation of the propagation from the first phase plate up to the second one is reported (Fig. 2(d.1-8)). Custom codes were developed in MatLab environment, based on the convolution algorithm applied to the Fresnel diffraction integral [43]. The phase patterns were

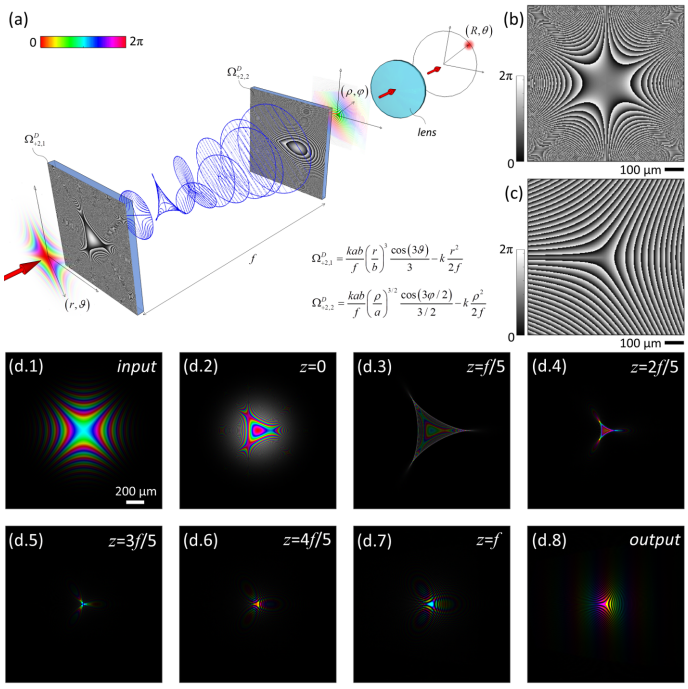

Fig. 2. Transformation of a multipole-phase beam of order m=+2. (a) Scheme: the input field is transformed by the first phase element imparting a circular-sector transformation with n=-1/2 and a final linear phase gradient is retained after the second phase element (performing the inverse circular sector transformation, i.e. n=-2). A lens is used for Fourier transform. Phase patterns of the first (b) and second (c) phase element, without the quadratic focusing (only the circular-sector transformation phase contribution is shown). Design parameters: a=500 μm, b=300 μm, f=10 mm, λ=632.8 nm, input beam waist w_0=312.5 μm. (d) Numerical simulation of the propagation of an input Gaussian beam carrying a multipole phase with m=+2, α=1.0·10^{-4} μm^{-2} (d.1) at different position on the z-axis, after illuminating the first element (d.2), up to the second optical element (d.3-d.7, f/5 step), and output phase-corrected beam (d.8). Colors and brightness refer to phase and intensity, respectively.

Optics EXPRESS

defined over a square mesh of 5633×5633 pixels with a spatial resolution of 312.5 nm. Input beams with different phase strengths and orientation angles are expected to generate linear phase gradients with different components of the wavevector on the plane, being focused at distinct positions on the back-focal plane of a lens. As shown in Fig. 3 for different phase strengths and orientations in input, the far-field spots are clearly distinguishable, enabling the detection of the input beams and the measurement of their carried energy. In Supplement 1 S3, the design and simulation of the multiplexing device are reported.

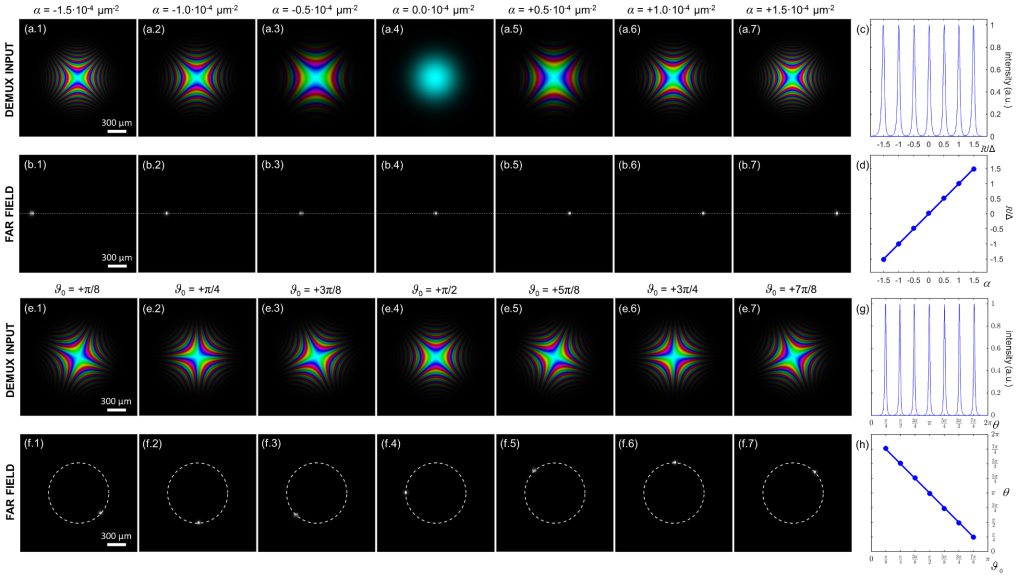

Fig. 3. Sorting of multipole-phase beams of order m=+2. Numerical simulations of different input beams with a multipole phase of order m=+2 entering the optical scheme depicted in Fig. 2. After applying the circular-sector transformation with n=-1/2, the multipole phase $\Phi^{in}{}_{2,j}=\alpha_j r^2\cos(2(\vartheta-\vartheta_{0,j}))$ of the jth beam is transformed into a linear phase $\Phi^{out}{}_{2,j}=\beta_j\rho\cos(\varphi-\varphi_{0,j})$, where $\beta_j=\alpha_j b^2/a$ and $\varphi_{0,j}=-2\vartheta_{0,j}$, and mapped to a point at the position $(R_j, \theta_j)=(f_F/k\,\beta_j, -2\vartheta_{0,j})$ at the back focal plane of a lens with focal length f_F. Design parameters of the transformation: a=500 μm, b=300 μm, f=10 mm, λ=632.8 nm, input waist w_0=312.5 μm. Focal length for far-field analysis: f_F=20 cm. (a.1-7) The beams are endowed with different strength parameter α in the set $\{0, \pm0.5, \pm1.0, \pm1.5\}\cdot10^{-4}$ μm^{-2}. As expected, a bright spot appears in the far field (b.1-7), at a position proportional to the input phase strength α. (c) Far-field cross-section on the white dashed line in (b). (d) Normalized spots position R/Δ ($\Delta= f_F/k\cdot b^2/a$) and theoretical trend (blue solid line) according to Eq. (6), as a function of the phase strength α [10^{-4} μm^{-2}]. (e.1-7) The beams are endowed with the same strength parameter α=+1.0·10^{-4} μm^{-2} and different rotation angles ϑ_0 from +π/8 to +7π/8, step +π/8. As expected, the bright spots appear over the same circle in far field at different angular positions equal to $-2\vartheta_0$ (f.1-7). (g) Far-field cross-section on the white dashed circle in (f). (h) Spots angular position θ and theoretical trend (blue solid line), as a function of the rotation angle ϑ_0.

3. Experimental test

The possibility to measure optically the parameters of a multipole-phase beams has been verified experimentally for illumination under beams of order m=+2. Multipole-phase beams were generated using a first LCoS spatial light modulator (SLM) (PLUTO-NIR-010-A, Holoeye) by applying a phase and amplitude modulation technique [44] (see Supplement 1 S6 for more details

Optics EXPRESS

on the technique). The SLM display was illuminated by a Gaussian beam ($\lambda = 632.8$ nm, beam waist w_0=240 μm, power 0.8 mW) emitted by a HeNe laser (HNR008R, Thorlabs), linearly polarized and expanded using a first telescope (f_1=2.54 cm, f_2=15.0 cm). A second telescope (f_3=20.0 cm, f_4=25.0 cm) was placed after the first SLM in order to isolate and image the first-order encoded mode onto a second LCoS SLM display (PLUTO-NIR-010-A, Holoeye) mounted on a 6-axis kinematic mount (K6XS, Thorlabs). A 50:50 beam-splitter was used to split the beam and check the input beam profile with a first CMOS camera (DCC1545M, Thorlabs). The orthogonality and orientation of the second SLM with respect to the incoming beam were carefully checked by acting on the knobs and goniometer of the 6-axis mount. The transformation optics imparting a circular-sector transformation with n=-1/2 was implemented with the second SLM, using the two halves of the display to upload the two distinct phase patterns, i.e., the transformer and the phase-corrector, and deploying a mirror for back-reflection as illustrated in the schemes in Fig. 4(b, c). This configuration reduces the degrees of freedom and simplifies the alignment procedure, as already shown in experimental implementations of *log-pol* diffractive sorters [29,45]. That is achieved by adding a phase term $\gamma_1 \cdot x$ to the first pattern, and centering the second element, i.e., the phase-corrector, at a distance $\gamma_1 f/k$ from the center of the first. Then, an additional spatial frequency carrier γ_2=1.5·γ_1 was added to the phase-corrector, in order to tilt the output beam out of its optical axis, as shown in the scheme in Fig. 4(a). In the specific, the experimental parameters chosen for the circular-sector transformation were a=1000 μm, b=1500 μm, and f=30 cm. The mirror was placed on a kinematic mount (KM100, Thorlabs) and its distance from the SLM display, equal to half the focal length of the first phase pattern, i.e. 15 cm, could be finely controlled with a micrometric translator (TADC-651, Optosigma). The SLM display was formed by 1920 × 1080 pixels of size 8 μm x 8 μm. Each phase pattern was designed inside a circle of radius $L/5 = 3.072$ mm, and the distance between the two centers was

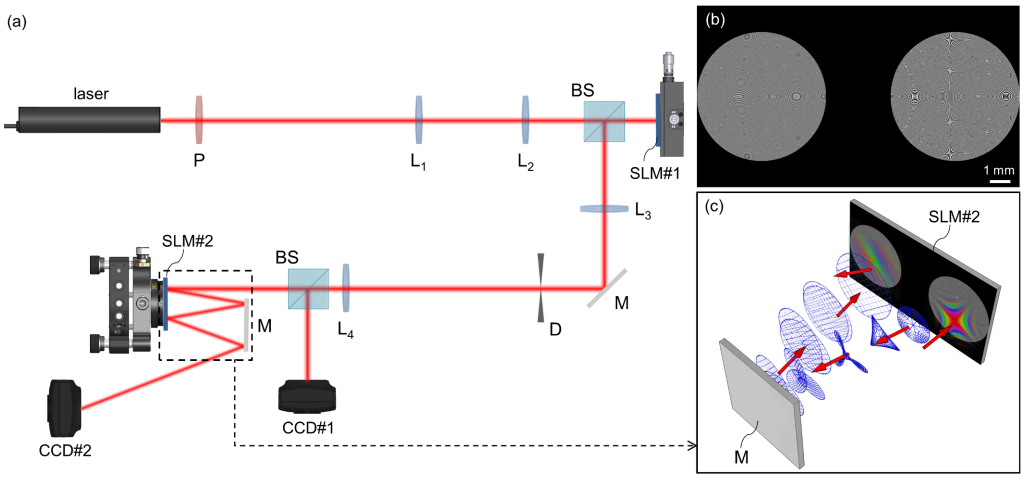

Fig. 4. Scheme of the experimental setup for optical tests. (a) The laser beam (λ=632.8 nm, waist size 240 μm) is linearly polarized (P) and expanded (f_1=2.54 cm, f_2=15.0 cm). A beam splitter (BS) is used to extract the back-reflected beam after phase/intensity reshaping with a first SLM (SLM#1) for multipole-phase generation. The beam is filtered (D) and resized (f_3=20.0 cm, f_4=25.0 cm) before illuminating a second SLM (SLM#2) on its first half implementing the circular-sector transformer. A mirror (M) is used for back-reflection on the second half of the display for phase correction (scheme in (c)). (b) Phase pattern uploaded on SLM#2: 1920 × 1080 pixels, pixel size 8 μm x 8 μm, 256 grey levels. A second beam splitter is used to check the beam intensity distribution on a first camera CCD#1. A second camera CCD#2 is placed on the focal plane of the phase-correcting pattern (f_F=40.0 cm).

Optics EXPRESS

set equal to $3L/5 = 9.216$ mm, being L the width of the SLM display. Finally, the transformed beam was collected by a second CMOS camera (DCC1545M, Thorlabs), placed on the focus of the phase-corrector pattern (f_F=40 cm).

As discussed in [28] for the *log-pol* case, the phase patterns in Eq. (5) are calculated in the stationary phase approximation for planar wavefronts, then they are expected to work perfectly only for collimated beams in input. Irrespective of their divergence, beams carrying multipole phases are not plane waves, and the local deviation due to the structured phase front is equal to $|\nabla\Omega^{(in)}|/k$. However, the optical transformation still works as expected, provided that the angular deviation introduced by the transformer dominates over any input deviation from normal incidence. For a given multipole order m, it is required that $|\nabla\Omega^{(in)}| << |\nabla\Omega^{D}{}_{1,m}|$, providing the condition $\alpha << kaw_0/(fmb^m)$, where w_0 is the input waist (Supplement 1 S4). For m=+2, we find $\alpha << kaw_0/(2fb^2)$, defining an upper threshold to the input strength that the system can measure without dramatic deviations.

The capability of the optical configuration to measure strength and orientation angle of multipole phases of order m=+2 was experimentally tested for input beams with a Gaussian intensity profile and a beam waist w_0=2.5 mm. With those given parameters of the optical

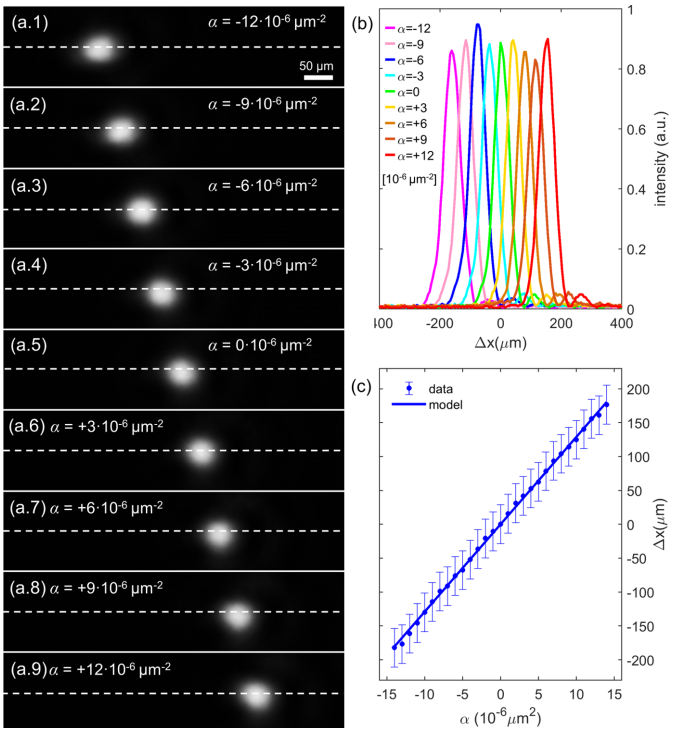

Fig. 5. Measurement of multipole-phase strength, m=+2. (a.1-9) Experimental output for varying multipole-phase strength α in the range from $-12\cdot10^{-6}$ µm^{-2} (a.1) to $+12\cdot10^{-6}$ µm^{-2} (a.9), step $3\cdot10^{-6}$ µm^{-2}, fixed orientation ϑ_0=0, and cross-sections (b) on the white dashed lines. (c) Far-field position as a function of the input strength α in the range from $-15\cdot10^{-6}$ µm^{-2} to $+15\cdot10^{-6}$ µm^{-2}, step $1\cdot10^{-6}$ µm^{-2}: experimental data (blue dots) and theoretical model (blue line). Error bar: half-width half-maximum. As expected, the shift of the far-field spot is proportional to the input strength α. Optical processing with n=-1/2 circular-sector transformation, design parameters: a=2000 µm, b=1000 µm, f=30 cm, f_F=40 cm, λ=632.8 nm. Theoretical slope: $\Delta_{th}=f_L b^2/(ka)=+20.14\cdot10^{+6}$ µm^3. Experimental slope: $\Delta_{exp}=+(20.20\pm0.08)\cdot10^{+6}$ µm^3.

Optics EXPRESS

transformation and input beam, the upper threshold for the measurable phase strength resulted around $8{\cdot}10^{-5}$ μm^{-2}, however significant deviations started to appear for values close to $2{\cdot}10^{-5}$ μm^{-2}. Therefore, we limited the analysis up to a maximum value of $1.5{\cdot}10^{-5}$ μm^{-2}. In Fig. 5, the output is reported for different values of the phase strength α at fixed orientation $\vartheta_0 = 0$. As expected, the far-field spots are arranged over the same line and they shift proportionally to α. Their positions exhibit a linear trend as a function of the input strength, and the value of the experimental slope $\Delta_{exp}=+(20.20 \pm 0.08){\cdot}10^{+6}$ μm^3 is in good agreement with the expected theoretical value $\Delta_{th}=f_L b^2/(ka)=+20.14{\cdot}10^{+6}$ μm^3. Then, we considered input beams with fixed multipole-phase strength $\alpha=+10{\cdot}10^{-6}$ μm^{-2} and varying rotation angle ϑ_0, increasing from $\vartheta_0=0$

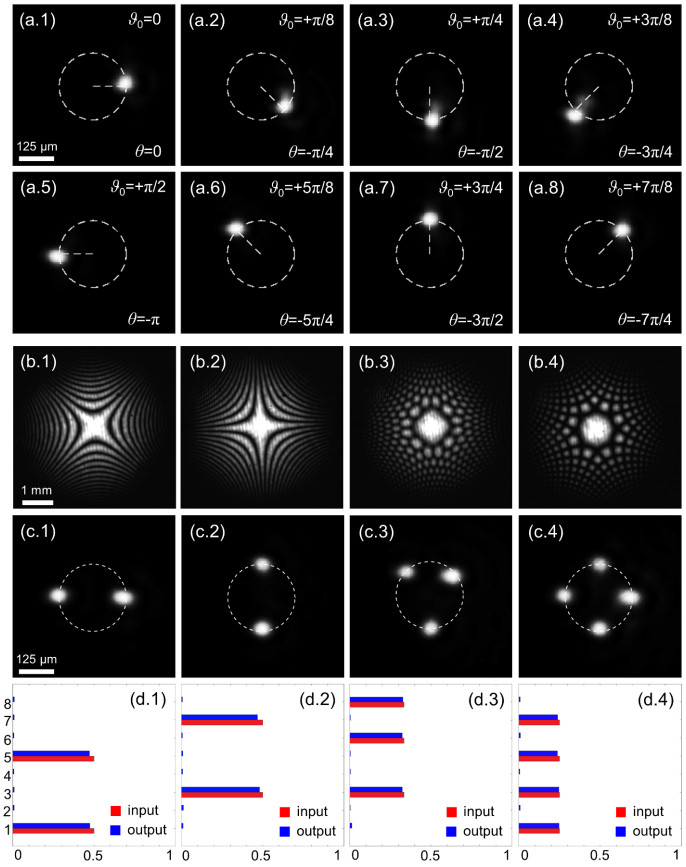

Fig. 6. Measurement and demultiplexing of multipole-phase orientation angle, m=+2. (a.1-8) Experimental output for varying multipole-phase orientation ϑ_0 in the range of 8 values from $\vartheta_0=0$ to $\vartheta_0=7\pi/8$, step $\pi/8$. Fixed phase strength $\alpha=+10{\cdot}10^{-6}$ μm^{-2}. Optical processing with n=-1/2 circular-sector transformation, design parameters: a=2000 μm, b=1000 μm, f=30 cm, f_F=40 cm, λ=632.8 nm. As expected, the output spots appear at the angular position $\theta=-2\vartheta_0$. The same set of beams has been used to test the demultiplexing capability of the system. (b.1-4) Intensity of the generated beams superposition, with orientation angles $\vartheta_0=0$ & $\vartheta_0=\pi/2$ (b.1), $\vartheta_0=\pi/4$ & $\vartheta_0=3\pi/4$ (b.2), $\vartheta_0=\pi/4$ & $\vartheta_0=5\pi/8$ & $\vartheta_0=7\pi/8$ (b.3), $\vartheta_0=0$ & $\vartheta_0=\pi/4$ & $\vartheta_0=\pi/2$ & $\vartheta_0=3\pi/4$ (b.4). (c.1-4) Experimental output after the demultiplexer. (d.1-4) Comparison between input (in red) and output (in blue) energy distributions over the selected range of channels. The jth channel corresponds to the input rotation angle $\vartheta_{0,j}=(j\text{-}1)\pi/8$. The total power has been normalized to unity.

Optics EXPRESS

at steps of $\Delta\vartheta_0 = \pi/8$. As shown in Figs. 6(a), the angular position θ of the output spots varies according to the relation $\theta = -2\vartheta_0$, as expected.

These results suggest the possibility to perform spatial-division multiplexing over a selected range of values of phase strengths and orientation angles. The values should be chosen properly in order to minimize the superposition of the corresponding spots in the far field, i.e., to reduce the cross-talk between the channels. In Fig. 6, experimental data are shown regarding the demultiplexing of several superpositions of multipole-phase beams endowed with the same phase strength $\alpha = +10 \cdot 10^{-6}$ μm^{-2} but different orientation angles in the set $\{\vartheta_{0,j} = (j-1)\pi/8\}$, $j = 1, \ldots, 8$. As expected, the optical system is able to sort the different contributions according to the parameters of the carried multipole phases.

4. Discussion

In a more general approach to the propagation of structured-phase beams, we introduced a novel framework based on even-unexploited beams carrying multipole harmonic phases. In the landscape of structured light, those beams present unique features in terms of compact all-optical multiplexing and sorting, solving straightforwardly the open issues of previous techniques. As a matter of fact, the steps of generation, propagation, and detection are here considered comprehensively for the first time in terms of conformal transformations of the wave fields, and the common ground is represented by the condition of harmonicity that the phases must satisfy. Although they are not modes in the strict sense, the existence of quasi-orthogonal multipole-phase patterns which are invariant under Fourier transform suggests the possibility to exploit those beams as distinct information carriers for spatial division multiplexing.

For a given multipole order m, the two continuous parameters describing phase strength and orientation angle define a 2D dense state space over which a set of quasi-orthogonal multipole-phase beams can be defined to carry distinct information channels over the same frequency. Although in principle any value of m can be chosen, the case $m = +2$ represents the ideal case for transmission, due to the conservation of the multipole order under Fourier transform, and the consequent symmetry between the multiplexing and demultiplexing devices. The core of those devices is represented by a conformal mapping between multipole phases and linear phase gradients, implemented by means of two confocal phase plates realizing a circular-sector transformation of factor $n = -1/m$. In the framework of optical vortices, those transformations were introduced to perform the multiplication and division of OAM in an efficient and compact manner [37]. In the present context, the same mapping has been applied for the measurement of structured beams endowed with multipole phases, representing a special and peculiar class of phase patterns with respect to the abovementioned transformation. While the sorting has been demonstrated using computer-controlled SLMs, the phase elements can be fabricated as diffractive optics [45] or in a metasurface form [38,46] and integrated into compact architectures, scaling straightforwardly to the more compact sizes considered in the simulation section.

The inter-channel cross-talk is related to the overlap between the far-field spots. Assuming a Gaussian-like intensity distribution with beam radius w_{out} for the beams exiting the phase-corrector, the spot size on the back-focal plane of the Fourier lens will be around $\lambda f_L / w_{out}$. Then, for given wavelength and focal length, it is possible to reduce the size of the far-field spots and consequently their mutual overlap, i.e., the cross-talk, acting on the size w_{out} of the beam, which is in turn related to the input one by the parameters a and b of the transformation ($w_{out} \approx a(w_{in}/b)^m$). However, the fields are expected not to exceed the size of the optical elements, which is dictated by the specific implementation and by the limits of the fabrication technique. Alternatively, the overlap between the far-field spots can be reduced acting on their mutual separation by increasing the corresponding phase strength values. For instance, as suggested in the previous section, a shorter focal length f of the transformation increases the phase strength threshold, enabling a

Optics EXPRESS

higher separation between the far-field spots without changing their size. The same considerations hold true, in reverse, when designing the multiplexer.

Conformal transformations represent an effective tool for wavefront manipulation and require only two confocal phase plates to perform a unitary transformation of the intensity and phase distributions of the input field. Thus, this method provides an all-optical solution for beam shaping which is more compact, feasible, and efficient than other techniques based for instance on holograms [22], on the cascade of many optical operations [23,25], or on integrated plasmonic or photonic platforms [26]. The key idea is to map conformally the structured wave fields into linear momentum states which can be practically generated or separated by using a Fourier lens. In the context of OAM beams, this has been performed by unwrapping the azimuthal phase gradient into a linear one using the *log-pol* mapping, which since its first implementation with SLM in 2010 [27], has known increasing improvements in miniaturization [31], resolution [29], and integration [45,46]. However, the axial-symmetry breaking and diffraction limitations still prevent a compact and efficient multiplexing of OAM beams, and additional optical elements, e.g., cylindrical lenses, are required for beam reshaping before and after the multiplexing and demultiplexing stages [31,32]. Moreover, the (de)multiplexing can be easily implemented only on one integer parameter, i.e., the azimuthal index ℓ, then the input/output channels are arranged along a fixed line. In order to exploit the full potential capacity offered by spatial multiplexing [47], an additional degree of freedom should be controlled besides OAM. However, the sorting on the radial number is not inherently included in the *log-pol* sorter, while it has been shown by adding further astigmatic elements [48] or by acting on the interference between the Gouy phases [49,50]. Moreover, the practical generation of multi-ring OAM beams with the inverse setup still remains a demanding task.

With respect to the *log-pol* sorter for OAM beams, the technique here presented outlines a more versatile implementation of the (de)multiplexing devices and automatically opens to a wider practical range of parameters. In fact, the parameters used to define a multipole phase, i.e., its strength α and rotation angle ϑ_0 on the plane, are continuous variables, and the only constraint on their choice is to avoid the overlapping of the corresponding bright spots at the detector stage, that is to guarantee a maximum threshold of cross-talk between them. In addition, the angular degree of freedom allows one to inherently cover the whole plane and to distribute the channels over a two-dimensional space. Furthermore, the output spots present a Gaussian-like intensity profile, avoiding the need for cumbersome beam reshaping. This is even more advantageous in the multiplexer design since the output beam of a standard source can illuminate the optics directly (Supplement 1 S3).

For positive multipole orders, the phase term is devoid of phase singularity, then it does not induce points of null intensity on the carrying beams, differently from the azimuthal phase of optical vortices. In those beams in fact, the out-of-axis component of the Poynting vector leads to a divergence of the vortex and to a consequent expansion of its dark center, which increases with the OAM value, affecting the efficiency of the receiver and limiting the application to short distances [51–55]. In Supplement 1, the simulated propagation of a multipole-phase beam with Gaussian intensity distribution is reported.

As far as guided propagation is concerned, beams with multipole phases are not exact solutions of the wave equation in the medium, then they should be properly described in terms of superposition of the fibre modes, with a consequent distortion of the input phase and intensity distributions due to the modal dispersion. On the other hand, due to the low modal dispersion and the self-imaging properties, graded-index (GRIN) fibres are expected to represent the best candidate for multipole-phase beams transmission [56]. For this reason, an immediate application of this spatial division multiplexing technique could be found in the field of data centers, where GRIN fibers are already deployed and the maximum distance length is around a few kilometers.

Optics EXPRESS

It is worth noting that the particular case of multipole phases of order m=+2 resembles the pattern of the well-known 2-fold astigmatisms. Then, the present method offers a solution to measure the amount and orientation of astigmatisms in a fast and direct way, and analogous schemes can be designed for higher order aberrations described by multipole phases with positive integer m (m-fold astigmatism) [57].

5. Conclusions

We envisage that the present work paves the way to a novel paradigm for spatial division multiplexing of structured phases. The optical schemes presented in this study outline the key configurations for the design of the multiplexing and demultiplexing devices required to implement a communication link, while the information carriers are provided by a defined set of multipole phases of the same order but with different strength and orientation values. The axial centered intensity makes this multiplexing configuration particularly interesting for free-space point-to-point communication, and its application can extend beyond the optical wavelengths. The exploitation of SDM has been acquiring increasing attention in the microwave range for next-generation free-space networks [58], where the realization of diffractive optics [59] and metasurfaces [60] for the control of the phase structure has recently been shown. Therefore, we envisage also the implementation of communication links in free-space based on a new generation of microwave diffractive antennas for the transmission and detection of multipole-phase beams in the microwave regime. Concurrently, these new beams are expected to provide novel complex field configurations for particle manipulation and light structuring, and new high-dimensional schemes for cryptographic applications at the single photon level.

Funding. CEPOLISPE, Italian Ministry of Defence (VORTEX 3).

Acknowledgments. This work was supported by project VORTEX 3 from CEPOLISPE. V.G. acknowledges Q-SORT, a project funded by the European Union's Horizon 2020 Research and Innovation Program under grant agreement No. 766970.

Disclosures. The authors declare no conflicts of interest.

Data availability. Data underlying the results presented in this paper are not publicly available at this time but may be obtained from the authors upon reasonable request.

Supplemental document. See Supplement 1 for supporting content.

References

1. H. Rubinstein-Dunlop, A. Forbes, M. V. Berry, M. R. Dennis, D. L. Andrews, M. Mansuripur, C. Denz, C. Alpmann, P. Banzer, T. Bauer, E. Karimi, L. Marrucci, M. Padgett, M. Ritsch-Marte, N. M. Litchinitser, N. P. Bigelow, C. Rosalez-Guzman, A. Belmonte, J. P. Torres, T. W. Neeley, M. Baker, R. Gordon, A. B. Stilgoe, J. Romero, A. G. White, R. Fickler, A. E. Willner, G. Xie, B. McMorran, and A. M. Weiner, "Roadmap on structured light," J. Opt. **19**(1), 013001 (2017).
2. L. Allen, M. W. Beijersbergen, R. J. C. Spreeuw, and J. P. Woerdman, "Orbital angular momentum of light and the transformation of Laguerre–Gaussian laser modes,"," Phys. Rev. A **45**(11), 8185–8189 (1992).
3. D. McGloin and K. Dholakia, "Bessel beams: diffraction in a new light," Contemp. Fisica **46**(1), 15–28 (2005).
4. C. Alpmann, C. Scholer, and C. Denz, "Elegant Gaussian beams for enhanced optical manipulation," Appl. Phys. Lett. **106**(24), 241102 (2015).
5. K. I. Willig, B. Harke, R. Medda, and S. W. Hell, "STED microscopy with continuous wave beams," Nat. Methods **4**(11), 915–918 (2007).
6. F. O. Fahrbach, V. Gurchenkov, K. Alessandri, P. Nassoy, and A. Rohrbach, "Self-reconstructing sectioned Bessel beams offer submicron optical sectioning for large fields of view in light-sheet microscopy," Opt. Express **21**(9), 11425–11440 (2013).
7. S. Jia, J. C. Vaughan, and X. Zhuang, "Isotropic three-dimensional super-resolution imaging with a self-bending point spread function," Nat. Photonics **8**(4), 302–306 (2014).
8. K. Dholakia and T. Cizmar, "Shaping the future of manipulation," Nat. Photonics **5**(6), 335–342 (2011).
9. M. Woerdemann, C. Alpmann, M. Esseling, and C. Denz, "Advanced optical trapping by complex beam shaping," Laser Photonics Rev. **7**(6), 839 (2013).
10. A. Sit, F. Bouchard, R. Fickler, J. Gagnon-Bischoff, H. Larocque, K. Heshami, D. Elser, C. Peutinger, K. Gunthner, B. Heim, C. Marquardt, G. Leuchs, R. W. Boyd, and E. Karimi, "High-dimensional intracity quantum cryptography with structured photons," Optica **4**(9), 1006–1010 (2017).

Optics EXPRESS

11. M. De Oliveira, I. Nape, J. Pinnell, N. TabeBordbar, and A. Forbes, "Experimental high-dimensional quantum secret sharing with spin-orbit-structured photons," Phys. Rev. A **101**(4), 042303 (2020).
12. G. Li, N. Bai, N. Zhao, and C. Xia, "Space-division multiplexing: the next frontier in optical communication," Adv. Opt. Photonics **6**(4), 413–487 (2014).
13. D. J. Richardson, J. M. Fini, and L. E. Nelson, "Space-division multiplexing in optical fibres," Nat. Photonics **7**(5), 354–362 (2013).
14. E. Agrell, M. Karlsson, A. R. Chraplyvy, D. J. Rochardson, P. M. Krummrich, P. Winzer, K. Roberts, J. K. Fisher, S. J. Savory, B. J. Eggleton, M. Secondini, F. R. Kschischang, A. Lord, J. Prat, I. Tomkos, J. E. Bowers, S. Srinivasan, M. Brandt-Pearce, and N. Gisin, "Roadmap of optical communications," J. Opt. **18**(6), 063002 (2016).
15. C. Brunet and L. A. Rusch, "Invited Paper: Optical fibers for the transmission of orbital angular momentum modes," Opt. Fiber Technol. **31**, 172–177 (2016).
16. A. E. Willner, Y. Ren, G. Xie, Y. Yan, L. Li, Z. Zhao, J. Wang, M. Tur, A. F. Molisch, and S. Ashrafi, "Recent advances in high-capacity free-space optical and radio-frequency communications using orbital angular momentum multiplexing," Phil. Trans. R. Soc. A. **375**(2087), 20150439 (2017).
17. H. Huang, G. Xie, Y. Yan, N. Ahmed, Y. Ren, Y. Yue, D. Rogawski, M. J. Willner, B. I. Erkmen, K. M. Birnbaum, S. J. Dolinar, M. P. J. Lavery, M. J. Padgett, M. Tur, and A. E. Willner, "100 Tbit/s free-space data link enabled by three-dimensional multiplexing of orbital angular momentum, polarization, and wavelength," Opt. Lett. **39**(2), 197 (2014).
18. M. Erhard, R. Flicker, M. Krenn, and A. Zeilinger, "Twisted photons: new quantum perspectives in high dimensions," Light: Sci. Appl. **7**(3), 17146 (2018).
19. J. Wang, "Twisted optical communications using orbital angular momentum," China Phys. Mech. Astron. **62**(3), 34201 (2019).
20. M. J. Padgett, "Orbital angular momentum 25 years on,"," Opt. Express **25**(10), 11265–11274 (2017).
21. A. M. Yao and M. J. Padgett, "Orbital angular momentum: origins, behavior and applications," Adv. Opt. Photonics **3**(2), 161–204 (2011).
22. G. Gibson, J. Courtial, M. J. Padgett, M. Vasnetsov, V. Pas'ko, S. M. Barnett, and S. Franke-Arnold, "Free-space information transfer using light beams carrying orbital angular momentum," Opt. Express **12**(22), 5448–5456 (2004).
23. J. Leach, M. J. Padgett, S. M. Barnett, S. Franke-Arnold, and J. Courtial, "Measuring the orbital angular momentum of a single photon," Phys. Rev. Lett. **88**(25), 257901 (2002).
24. G. Labroille, B. Denolle, P. Jian, P. Genevaux, N. Treps, and J.-F. Morizur, "Efficient and mode selective spatial mode multiplexer based on multi-plane light conversion," Opt. Express **22**(13), 15599–15607 (2014).
25. N. K. Fontaine, R. Ryf, H. Chen, D. Neilson, and J. Carpenter, "Design of high order mode-multiplexers using multiplane light conversion," in *Proc. European Conference on Optical Communication (ECOC)* (2017).
26. T. Su, R. P. Scott, S. S. Djordjevic, N. K. Fontaine, D. J. Geisler, X. Cai, and S. J. B. Yoo, "Demonstration of free space coherent optical communication using integrated silicon photonic orbital angular momentum devices," Opt. Express **20**(9), 9396–9402 (2012).
27. G. C. G. Berkhout, M. P. J. Lavery, J. Courtial, M. W. Beijersbergen, and M. J. Padgett, "Efficient sorting of orbital angular momentum states of light," Phys. Rev. Lett. **105**(15), 153601 (2010).
28. M. P. J. Lavery, D. J. Robertson, A. Sponselli, J. Courtial, N. K. Steinhoff, G. A. Tyler, A. E. Willner, and M. J. Padgett, "Efficient measurement of an optical orbital-angular-momentum spectrum comprising more than 50 states," New J. Phys. **15**(1), 013024 (2013).
29. G. Ruffato, M. Girardi, M. Massari, E. Mafakheri, B. Sephton, P. Capaldo, A. Forbes, and F. Romanato, "A compact diffractive sorter for high-resolution demultiplexing of orbital angular momentum beams," Sci. Rep. **8**(1), 10248 (2018).
30. R. Fickler, R. Lapkiewicz, M. Huber, M. P. J. Lavery, M. J. Padgett, and A. Zeilinger, "Interface between path and orbital angular momentum entanglement for high-dimensional photonic quantum information," Nat. Commun. **5**(1), 4502 (2014).
31. G. Ruffato, M. Massari, G. Parisi, and F. Romanato, "Test of mode-division multiplexing and demultiplexing in free-space with diffractive transformation optics," Opt. Express **25**(7), 7859–7868 (2017).
32. W. Li, K. S. Morgan, Y. Li, K. Miller, G. White, R. J. Watkins, and E. G. Johnson, "Rapidly tunable orbital angular momentum (OAM) system for higher order Bessel beams integrated in time (HOBBIT)," Opt. Express **27**(4), 3920–3934 (2019).
33. Y. Wen, I. Chremmos, Y. Chen, J. Zhu, Y. Zhang, and S. Yu, "Spiral transformation for high-resolution and efficient sorting of vortex modes," Phys. Rev. Lett. **120**(19), 193904 (2018).
34. Y. Wen, I. Chremmos, Y. Chen, Y. Zhang, and S. Yu, "Arbitrary multiplication and division of the orbital angular momentum of light," Phys. Rev. Lett. **124**(21), 213901 (2020).
35. Y. Guo, S. Zhang, M. Pu, Q. He, J. Jin, M. Xu, Y. Zhang, P. Gao, and X. Luo, "Spin-decoupled metasurface for simultaneous detection of spin and orbital angular momenta via momentum transformation," Light: Sci. Appl. **10**(1), 63 (2021).
36. S. Takashima, H. Kobayashi, and K. Iwashita, "Integer Multiplier for Orbital Angular Momentum of Light using Circular-Sector Transformation," Phys. Rev. A **100**(6), 063822 (2019).
37. G. Ruffato, M. Massari, and F. Romanato, "Multiplication and division of the orbital angular momentum of light with diffractive transformation optics," Light: Sci. & Appl. **8**(1), 113 (2019).

Optics EXPRESS

38. G. Ruffato and F. Romanato, "Design of continuously-variant metasurfaces for conformal transformation optics," Opt. Express **28**(23), 34201–34218 (2020).
39. M. Born and E. Wolf, *Principles of optics* (Pergamon Press, 1980).
40. O. Bryngdahl, "Geometrical transformations in optics," J. Opt. Soc. Am. **64**(8), 1092–1099 (1974).
41. W. J. Hossack, A. M. Darling, and A. Dahdouh, "Coordinate transformations with multiple computer-generated optical elements," J. Mod. Opt. **34**(9), 1235–1250 (1987).
42. G. Ruffato, E. Rotunno, L. M. C. Giberti, and V. Grillo, "Arbitrary conformal transformations of wave functions," Phys. Rev. Appl. **15**(5), 054028 (2021).
43. J. Li, Z. Peng, and Y. Fu, "Diffraction transfer function and its calculation of classic diffraction formula," Opt. Commun. **280**(2), 243–248 (2007).
44. C. Rosales-Guzmán and A. Forbes, *How to shape light with spatial light modulators* (SPIE SPOTLIGHT, 2017).
45. G. Ruffato, M. Massari, M. Girardi, G. Parisi, M. Zontini, and F. Romanato, "Non-paraxial design and fabrication of a compact OAM sorter in the telecom infrared," Opt. Express **27**(17), 24123–24134 (2019).
46. G. Ruffato, P. Capaldo, M. Massari, E. Mafakheri, and F. Romanato, "Total angular momentum sorting in the telecom infrared with silicon Pancharatnam-Berry transformation optics," Opt. Express **27**(11), 15750–15764 (2019).
47. N. Zhao, X. Li, G. Li, and J. M. Kahn, "Capacity limits of spatially multiplexed free-space communication," Nat. Photonics **9**(12), 822–826 (2015).
48. A. Dudley, T. Mhlanga, M. Lavery, A. McDonald, F. S. Roux, M. Padgett, and A. Forbes, "Efficient sorting of Bessel beams," Opt. Express **21**(1), 165–171 (2013).
49. Y. Zhou, M. Mirhosseini, D. Fu, J. Zhao, S. M. H. Rafsanjani, A. E. Willner, and R. W. Boyd, "Sorting photons by radial quantum number," Phys. Rev. Lett. **119**(26), 263602 (2017).
50. D. Fu, Y. Zhou, R. Qi, S. Oliver, Y. Wang, S. M. H. Rafsanjani, J. Zhao, M. Mirhosseini, Z. Shi, P. Zhang, and R. W. Boyd, "Realization of a scalable Laguerre–Gaussian mode sorter based on a robust radial mode sorter," Opt. Express **26**(25), 33057–33065 (2018).
51. A. E. Willner, G. Xie, L. Li, Y. Ren, Y. Yan, N. Ahmed, Z. Zhao, Z. Wang, C. Liu, and A. J. Willner, "Design challenges and guidelines for free-space optical communication links using orbital-angular-momentum multiplexing of multiple beams," J. Opt. **18**(7), 074014 (2016).
52. G. Xie, L. Li, Y. Ren, H. Huang, Y. Yan, N. Ahmed, Z. Zhao, M. P. J. Lavery, N. Ashrafi, S. Ashrafi, R. Bock, M. Tur, A. F. Molish, and A. E. Willner, "Performance metrics and design considerations for a free-space optical orbital-angular-momentum multiplexed communication link," Optica **2**(4), 357–365 (2015).
53. L. Li, R. Zhang, P. Liao, H. Song, K. Zou, G. Xie, Z. Zhao, C. Liu, H. Song, K. Pang, A. N. Willner, A. Almaiman, D. Starodubov, B. Lynn, R. Bock, M. Tur, and A. E. Willner, "Limited-size aperture effects in an orbital-angular-momentum-multiplexed free-space optical data link between a ground station and a retro-reflecting UAV," Opt. Commun. **450**, 241–245 (2019).
54. R. Chen, H. Zhou, M. Moretti, X. Wang, and J. Li, "Orbital angular momentum waves: generation, detection, and emerging applications," IEEE Commun. Surv. Tutorials **22**(2), 840–868 (2020).
55. F. Zheng, Y. Chen, S. Ji, and G. Duan, "Research status and prospects of orbital angular momentum technology in wireless communication," Prog. Electromagn. Res. **168**, 113–132 (2020).
56. G. P. Agrawal, "Self-imaging in multimode graded-index fibers and its impact on nonlinear phenomena," Opt. Fiber Technol. **50**, 309–316 (2019).
57. R. Brydson, *Aberration-corrected analytical transmission electron microscopy* (John Wiley & Sons, First edition, 2011).
58. I. B. Djordjevic, "OAM-based hybrid free-space optical-terahertz multidimensional coded modulation and physical-layer security," IEEE Photonics J. **9**(4), 1–12 (2017).
59. C. Liu, X. Wei, L. Niu, K. Wang, Z. Yang, and J. Liu, "Discrimination of orbital angular momentum modes of the terahertz vortex beam using a diffractive mode transformer," Opt. Express **24**(12), 12534–12541 (2016).
60. H. Zhao, B. Quan, X. Wang, C. Gu, J. Li, and Y. Zhang, "Demonstration of orbital angular momentum multiplexing and demultiplexing based on a metasurface in the terahertz band," ACS Photonics **5**(5), 1726–1732 (2018).